

Simultaneous Localization and Mapping with Power Network Electromagnetic Field

Chris Xiaoxuan Lu
University of Oxford
xiaoxuan.lu@cs.ox.ac.uk

Yang Li*
Shenzhen University
yli@szu.edu.cn

Peijun Zhao
University of Oxford
peijun.zhao@cs.ox.ac.uk

Changhao Chen
University of Oxford
chencch852@gmail.com

Linhai Xie
University of Oxford
linhai.xie@cs.ox.ac.uk

Hongkai Wen
University of Warwick
hongkai.wen@dcs.
warwick.ac.uk

Rui Tan
Nanyang Technological
University
tanrui@ntu.edu.sg

Niki Trigoni
University of Oxford
niki.trigoni@cs.ox.ac.uk

ABSTRACT

Various sensing modalities have been exploited for indoor location sensing, each of which has well understood limitations, however. This paper presents a first systematic study on using the electromagnetic field (EMF) induced by a building's electric power network for simultaneous localization and mapping (SLAM). A basis of this work is a measurement study showing that the power network EMF sensed by either a customized sensor or smartphone's microphone as a side-channel sensor is spatially distinct and temporally stable. Based on this, we design a SLAM approach that can reliably detect loop closures based on EMF sensing results. With the EMF feature map constructed by SLAM, we also design an efficient online localization scheme for resource-constrained mobiles. Evaluation in three indoor spaces shows that the power network EMF is a promising modality for location sensing on mobile devices, which is able to run in real time and achieve sub-meter accuracy.

CCS CONCEPTS

• **Human-centered computing** → **Ubiquitous and mobile computing**; • **Hardware** → *Sensor applications and deployments*;

*This work was completed while Yang Li was with Advanced Digital Sciences Center, Illinois at Singapore.

Permission to make digital or hard copies of all or part of this work for personal or classroom use is granted without fee provided that copies are not made or distributed for profit or commercial advantage and that copies bear this notice and the full citation on the first page. Copyrights for components of this work owned by others than ACM must be honored. Abstracting with credit is permitted. To copy otherwise, or republish, to post on servers or to redistribute to lists, requires prior specific permission and/or a fee. Request permissions from permissions@acm.org.

MobiCom '18, October 29-November 2, 2018, New Delhi, India

© 2018 Association for Computing Machinery.

ACM ISBN 978-1-4503-5903-0/18/10...\$15.00

<https://doi.org/10.1145/3241539.3241540>

KEYWORDS

Electromagnetic field sensing; Power line network; Simultaneous localization and mapping; Indoor localization

ACM Reference Format:

Chris Xiaoxuan Lu, Yang Li, Peijun Zhao, Changhao Chen, Linhai Xie, Hongkai Wen, Rui Tan, and Niki Trigoni. 2018. Simultaneous Localization and Mapping with Power Network Electromagnetic Field. In *The 24th Annual International Conference on Mobile Computing and Networking (MobiCom '18), October 29-November 2, 2018, New Delhi, India*. ACM, New York, NY, USA, 16 pages. <https://doi.org/10.1145/3241539.3241540>

1 INTRODUCTION

Recent years have seen the increasing need of location awareness by mobile applications. As of November 2017, 62% of the top 100 free Android Apps on Google Play require location services. While GPS can provide outdoor locations with satisfactory accuracy, indoor location sensing for mobiles has been a hard problem. Research in the last two decades has exploited various sensing modalities for indoor location sensing. Examples include various radio frequency (RF) signals (e.g., WiFi [11, 16, 50, 51], GSM [17], FM radio [6]), visible light [49, 52, 55], imaging [10, 13, 14, 54], acoustics [41], and geomagnetism [12, 18, 22, 35, 36, 44]. However, each sensing modality bears some limitations. RF signals have changeable propagation paths and received signal strengths (RSSes) due to barriers and transmitters' dynamic power control. Visual lights are vulnerable to blockage. Imaging is power demanding and privacy breaching. Geomagnetic sensing is susceptible to change of altitude.

This paper explores a new modality for indoor location sensing, i.e., the ambient electromagnetic fields (EMFs) generated by the electric power networks in civil infrastructures. These power networks supply alternating current (ac) voltages with an effective value of 220 V or 110 V in a nominal frequency of 50 Hz or 60 Hz to the electric appliances distributed in the buildings. As a result, the electromagnetic

radiations (EMRs) from the powerlines in a building will form an ambient EMF. The noises induced by the power network EMF at electronic devices, called *mains hums*, are undesirable in general and often removed by the devices' built-in filters. However, recent studies leveraged the periodic and synchronous properties of the mains hums to design clock synchronization approaches for indoor sensors [33] and wearables [48]. Moreover, a study in [23] shows that the mains hums sensed by indoor mote-class sensors carry time information with sub-second resolution, due to the subtle but spatially homogeneous imperfections in the mains hum's periodicity. While the powerline EMR's time-related properties have been the focus of existing studies, the spatial properties of power network EMF and whether these properties can be exploited for indoor location sensing have received no systematic research.

Hypothetically, as the powerline EMR intensity decays with the physical distance from the emitting powerline, the power network EMF formed by the superposition of the EMRs from the permanent powerlines running in the building infrastructures will give a spatially distinct but temporally stable intensity field, which is a basis for location sensing. To verify our intuition, we use two types of sensors, i.e., a customized EMR receiver and smartphone microphone, to conduct extensive measurements in various buildings. The EMR receiver is based on a tank circuit tuned to the power network's nominal frequency, while the smartphone microphone can perform side-channel sensing due to the leaked mains hum in audio recordings. Our measurement results confirm positively our hypothesis in the domain of indoor pedestrian walkways. In particular, compared with geomagnetic fields that often show altitude-varying intensity, power network EMFs exhibit better altitude-invariability, suggesting that the power network EMF-based location sensing can be less susceptible to user height.

Based on the measurement study, we design a Simultaneous Localization and Mapping (SLAM) approach exploiting the unique characteristics of power network EMF. Our approach jointly estimates both the user locations and the power network EMF feature map of the workspace, without labor-intensive surveying or fingerprinting. The constructed power network EMF feature map is metrically consistent, where locations are associated with corresponding power network EMF signatures. In particular, we bespoke our SLAM approach for the power network EMF modality, and design novel loop closure detection and curation algorithms to reliably recognize previously visited locations from the observed power network EMF signals. This is of crucial importance for SLAM using power network EMF, as standard techniques (e.g. directly comparing the EMF signals at different locations) would produce many false positive loop closure proposals,

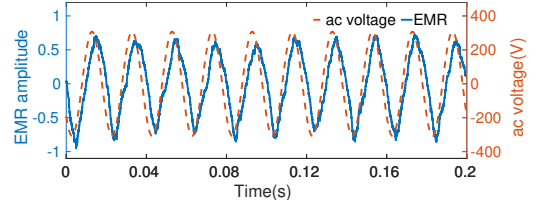


Figure 1: The normalized EMR amplitude around a live wire and the ac voltage between the live wire and the neutral wire.

and thus significantly jeopardize the consistency of the feature map and deteriorate localization performance. Given the constructed power network EMF feature map, we also design an efficient online localization scheme capable of positioning the user in real time on resource-constrained devices.

We evaluate the proposed SLAM approach in realistic indoor/semi-outdoor environments including a lab space, an office building and a shopping center. The evaluation shows that, (i) with the customized EMR sensor, we can construct the power network EMF feature maps with sub-meter accuracy, and achieve meter level localization with the registered maps, (ii) on commercially off-the-shelf (COTS) platforms, the composite modality of geomagnetism and power network EMF (sensed through microphone) can have comparable performance, and (iii) by exploiting unique properties of power network EMF including its stability and smoothness, we could achieve real-time localization (0.69 s per measurement) on embedded platforms.

The remainder of this paper is organized as follows. §2 introduces the background of powerline EMR sensing. §3 presents a measurement study. §4 presents the details of the power network EMF-based SLAM and localization approaches. §5 presents the evaluation results. §6 reviews related work. §7 concludes.

2 POWERLINE EMR SENSING

2.1 Background

The EMR around an ac powerline is a composite effect of the time-varying electric field generated by the line's ac voltage and the magnetic field generated by the ac current going through the line. Fig. 1 shows the readings of an EMR reception device (cf. §2.2) placed close to a 220 V 50 Hz live wire and the corresponding ac voltage between the live wire and the neutral wire. We can see that the EMR follows the ac voltage well. A modern civil infrastructure often has massive powerlines running in the walls, above ceilings, below floors, to power various appliances distributed in the indoor space. The intensity of the EMR attenuates with the distance from the line, where the attenuation can be modeled by the power law. As a result, those many powerlines in the infrastructure

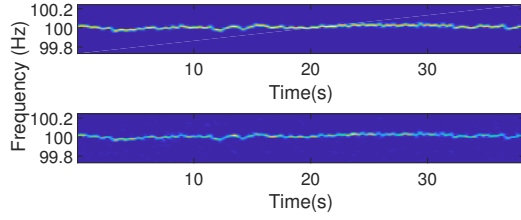


Figure 2: The 2nd harmonic of the powerline EMRs sensed by an EMR sensor (upper) and a smartphone microphone (lower). The smartphone can capture the 2nd harmonic faithfully.

will generate an EMF that has a sophisticated spatial intensity distribution over the indoor space, which highly depends on the routing of the powerlines. It is thus of great interest that whether the power network EMF has the spatial distinctness and temporal stability properties desired by location sensing.

Electromagnetic emanations from building power networks have been exploited in several applications. For instance, in a circuit seeker system [2], an injector injects modulated signals into a power outlet and then a seeker can identify the routing of nearby embedded powerlines by sensing the corresponding powerline EMR. A building’s power network can also be used as an effective AM radio antenna [1], because the size of a building can be close to AM radio wavelengths (i.e., hundreds meters). Different from these existing applications that use the building power networks to emit certain waves, this paper inquiries whether the power network EMF, an inevitable side effect of electricity delivery, can be exploited for location sensing.

2.2 Powerline EMR Reception

We use following two techniques to sense powerline EMR.

Customized Powerline EMR Sensor: We build a powerline EMR sensor consisting of a tank circuit and a signal amplifier. Our design uses a combination of a 470 mH coil inductor and a 22 μ F capacitor, to achieve a resonance frequency of 50 Hz (i.e., the power network frequency in our region). By using a 15 μ F capacitor, the tank circuit can be tuned to 60 Hz, which is the nominal frequency in Americas. A two-stage amplification circuit is applied to amplify the μ V-level output of the tank circuit to a volt-level input to an analog-to-digital converter mounted on a Raspberry Pi board. Our customized powerline EMR sensor can be readily integrated with various robot and drone platforms.

Side-channel Sensing by Microphone: The internal of a microphone is a capacitor consisting of a membrane and a metal conductor. The vibration of the membrane in response to sound results in time-varying capacitance between the

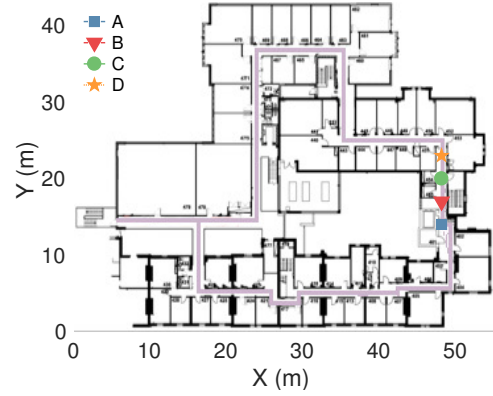


Figure 3: Test points (A, B, C, D) and walking trajectories (in thistle color) in an office building.

membrane and the metal conductor, which is translated to a voltage signal. The power network EMF can induce a time-varying voltage across the metal conductor, resulting in the mains hum in audio recordings. The mains hum can be extracted using a band-pass filtering algorithm. In this paper, we use smartphones’ built-in microphones and extract the mains hum and its harmonics. Fig. 2 shows the frequency of the second harmonic sensed by a customized powerline EMR sensor and a smartphone microphone. We can see that the smartphone can capture the second harmonic faithfully.

The results based on the above two types of sensors will provide insights into the limits of power network EMF-borne spatial information and practicality of power network EMF-based location sensing on COTS mobile platforms.

3 MEASUREMENT STUDY

We conduct experiments to investigate whether the power network EMF has the properties desired for location sensing.

3.1 Power Network EMF’s Spatial Distinctness

This set of experiments investigates whether the power network EMF intensities at different locations in an indoor space are distinct. We use the customized powerline EMR sensors to perform measurements in an office building with an area of about 2,475 m². Fig. 3 shows the floor plan. We set the sampling rate of our sensors to 8 kHz and applied a 5-step moving filter to remove high-frequency noises in the sampled signals.

Basic Time/Frequency Characteristics: We place our powerline EMR sensors at four locations in a corridor by every three meters, which are marked by A, B, C, and D in Fig. 3. Fig. 4(a) shows the power spectral densities of the power network EMF intensities collected at the four locations. We

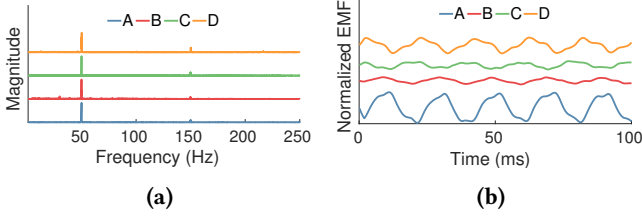


Figure 4: Time/frequency Characteristics. (a) Power spectral density. (b) 100 ms signal snippets. The curves in the figures are vertically displaced for better visual comparison among them.

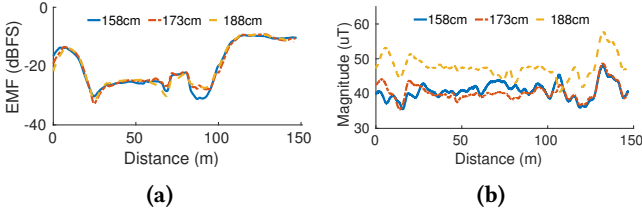


Figure 5: Power network EMF's invariability and geomagnetic field's variability with user height. (a) Power network EMF. (b) Geomagnetic field.

can see that they have similar characteristics, i.e., the sensed signal consists of a 50 Hz major component and several harmonics. Fig. 4(b) shows the 100 ms snippets of the sensed signals at the four locations in the same time duration. The power network EMF intensities at different locations have distinct waveforms and amplitudes. This distinctness is consistent with our understanding, as power network EMF has a spatial distribution. As discussed in §2.1, this distribution mainly depends on the routing of the powerlines. As the powerline routing usually stays fixed, the spatially distributed power network EMF is promising for location sensing.

Invariability with User Height: The spatial distinctiveness of indoor geomagnetic signals has been studied [8, 15]. Power network EMF and geomagnetic field are different. Geomagnetic field is the magnetic field that extends from the Earth's interior out into space. Due to the metal infrastructure in the buildings, geomagnetic field is distorted in indoor environments and can be utilized as the location signature. Geomagnetic intensity is static over time. In contrast, the power network EMF emitted from the ac powerlines is a time-varying field. Our following measurements show that, compared with the geomagnetic field, the power network EMF exhibits better invariability with user height.

We recruit three users with different heights (158cm, 173cm, and 188cm) who carry our powerline EMR sensor and a smartphone, and walk in a 150-meter pathway in a building.

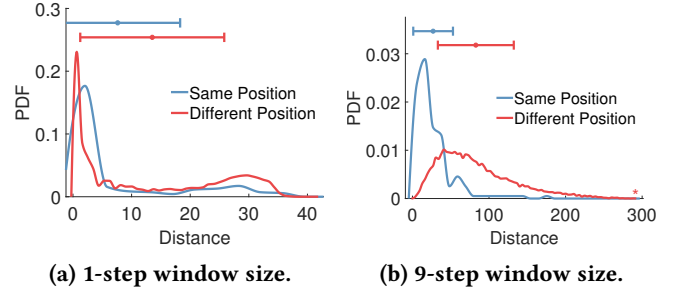


Figure 6: Distributions of DTW distance between two power network EMF RMS segments at the same or different locations.

Fig. 5 shows the root mean square (RMS) value measured by our powerline EMR sensor and the geomagnetic magnitude measured by the phone's 3-axis magnetometer. Each RMS value is computed based on readings in a 20 ms window. Though both sensing modalities are affected by the sensor altitude, the geomagnetic sensing is apparently more susceptible as the envelope of the geomagnetic magnitude varies much with user height. In contrast, the envelope of the power network EMF RMS exhibits better invariability against user height. This result implies that the power network EMF signature map can be constructed based on data crowd-sourced from users with different heights.

Location Discriminability: This set of experiments investigates whether we can discriminate different locations in the resolution of footsteps based on power network EMF measurement traces. A researcher carrying a powerline EMR sensor and a smartphone walks three loops along the trajectory showed in Fig 3. This trajectory covers all the pathways in the building. We compute the sensed signal's RMS trace and divide it into non-overlap segments, where a segment corresponds to a footstep sensed by the smartphone's inertial measurement units (IMUs). As the segments may have different lengths due to varying walking speed and pattern, we use the dynamic time warping (DTW) to measure the similarity between any two segments. Fig. 6a shows the distributions of the DTW distance between any two segments collected at the same location or different locations, respectively. The two distributions largely overlap, suggesting that the power network EMF RMS with a segmentation window size of one footstep is not location-discriminative. Differently, if we segment the power network EMF RMS trace with a segmentation window of nine footsteps, as shown in Fig. 6b, the two distributions become less overlapped. This means that with the 9-step window size, though not ideal, the location discriminability of power network EMF can be potentially exploited by SLAM. In §4, we will explain how the proposed SLAM approach can reliably distinguish the

same or different locations with the observed power network EMF signals in more detail.

3.2 Power Network EMF's Temporal Stability

This section investigates the temporal stability of the power network EMF. Although conventional SLAM systems only require short-term stability of loop-closure landmarks, long-term stability is still desirable, because the constructed feature maps can be reused for user navigation afterwards.

Impact of Individual Electric Appliances: Operating status changes of electric appliances causes varying ac currents in powerlines and therefore varying magnetic field. We conduct a set of controlled experiments to investigate the impact of the on/off operating statuses of individual electric appliances on the measurements of a powerline EMR sensor. Fig. 10a shows the power network EMF amplitude in decibels relative to full scale (dBFS) measured at different distances from an electric appliance when it is on and off. We can see that the operating statuses of the appliances can affect the power network EMF measurements. However, the impact is less than 1 dBFS when the sensor is more than one meter from the appliance. This is because that the magnetic intensity attenuates with distance and the measurement of the sensor is dominated by the superposition of the EMRs from all powerlines in the building compared with the EMR contributed by the tested appliance. Among the eight tested appliances, the operating status changes of the dryer, the microwave, and the fridge introduce considerable impact on the sensor measurements in their near fields. However, the near fields of these appliances are generally limited compared with the walking areas of built environments. From the measurement results, we can observe that switching off some appliances may increase the measurements at certain distances. This is because these appliances make negative contributions to the EMR superposition at those distances.

Impact of Near-by Human Bodies: A researcher holds a powerline EMR sensor and stands still at an indoor location. Then, more persons join the experiment by standing still about 0.5 m from the researcher. Fig. 8 shows the error bars of the sensor measurements when different numbers of persons stand around the researcher. We can see that the nearby human bodies have little impact on the sensor measurements. Unlike the short-wavelength RF signals (e.g., WiFi) that are susceptible to barriers, the 50 Hz EMR signal has an extremely long wavelength and thus are not affected by small-size barriers like human bodies.

Temporal Stability: We deploy four customized powerline EMR sensors at four different fixed locations in two countries

for 14 days. Each sensor records power network EMF intensities for one minute every two hours. Fig. 10a shows the error bars of each sensor's measurements in the one-minute duration. We can see that their measurements are stable over time. For comparison, Fig. 9 shows a smartphone's WiFi RSS values for a number of access points over 24 hours. We can clearly see the temporal variations of the WiFi RSS.

We also measure the power network EMF intensity when traversing a loop along the trajectory shown in Fig. 3 in a winter and the following summer. Fig. 10b plots the power network EMF RMS traces in the two seasons. As the building shown in Fig. 3 is located in the Temperate Zone, the electric loadings of the building in winter and summer are different. However, as shown in Fig. 10b, the power network EMF traces in the two seasons are desirably similar. This suggests that the ac voltage is the major exciter of the power network EMF, rather than the loading-dependent current. The above results show the power network EMF's temporal stability in the tested sites, and imply that once a power network EMF fingerprint database is developed through SLAM, it can be used for localization in considerably long time periods. In case of building infrastructure changes and/or powerline rerouting, it is readily for existing crowd-sourcing localization tools to update the database timely.

3.3 Location Discriminability of Power Network EMF Sensed by Smartphone

Phone's Power Network EMF Sensing Performance: As microphone is a side-channel sensor, we assess the impact of various daily life sounds on its power network EMF sensing. A Huawei P9 phone is placed at a fixed location to record audio for five minutes. Meanwhile, we intentionally create various interfering sounds, i.e., music and human speech that are most probably faced by SLAM/localization systems for pedestrians. Fig. 11 shows the distributions of the normalized intensity of the 50 Hz mains hum and its harmonics. From the figure, we can see that the music and human speech have larger impact on the 150 Hz harmonic, compared with the 50 Hz mains hum and the 100 Hz harmonic. This is because the 150 Hz harmonic collides with some human voice components. Although human voice can be down to 80 Hz [32] and collides with the 100 Hz harmonic, such cases are rare. As some high-end phones can effectively suppress the 50 Hz mains hum, we adopt the 100 Hz harmonic only, unless we need multiple harmonics to improve performance (cf. §4.4).

Mitigating Inefficacy of Geomagnetism-based Sensing: A researcher carries the Huawei P9 phone and walks three loops along the trajectory shown in Fig. 3. The phone's magnetometer and microphone continuously record geomagnetic and power network EMF data traces. This section

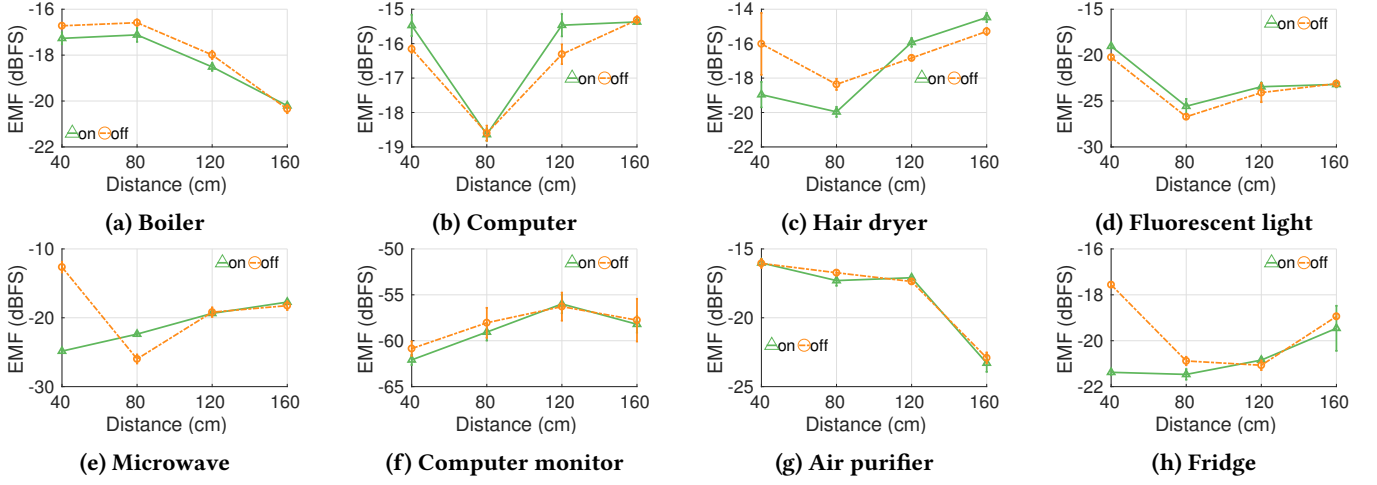


Figure 7: Impact of individual electric appliances on power network EMF sensing.

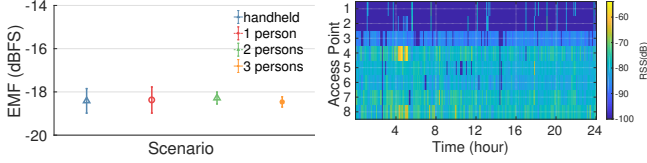


Figure 8: Nearby human body impact.

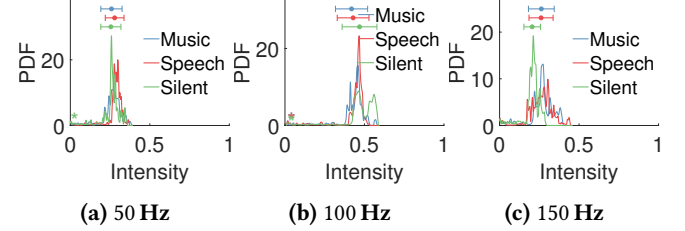


Figure 11: Power network EMF captured by a smart-phone microphone.

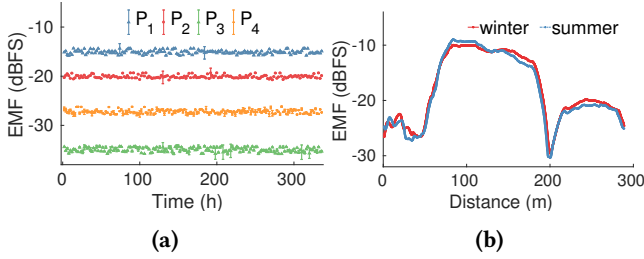


Figure 10: Temporal stability. (a) The power network EMF amplitude measured at four fixed locations in two countries over 14 days. The measurements labeled by P_1 and P_2 are obtained in country A; these labeled by P_3 and P_4 are obtained in country B. (b) The power network EMF amplitude trace when a researcher carrying the sensor walks along the same trajectory shown in Fig. 3 in a winter and the following summer.

particularly investigates the feasibility of using microphone-sensed EMF to mitigate the localization inefficient points by geomagnetic sensing. The insight for the mitigation is that when geomagnetic features are less discriminative (small gap) and insufficient to differentiate locations, power network EMF sensing can help enhance location distinctions,

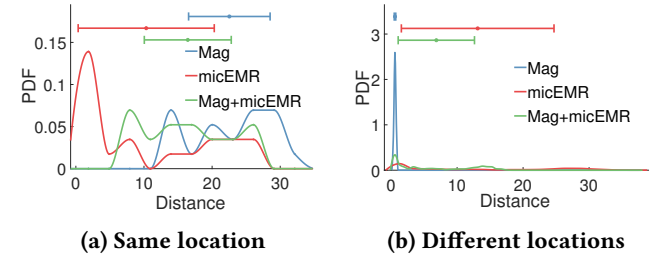


Figure 12: DTW distance distributions of various modalities at the same and different locations.

sensed with a COTS microphone. The vice is versa for inefficient cases of same locations. To account for the varying walking speeds in data collection, we use dynamic time warping (DTW) to calculate the distance between sequences for both geomagnetic and EMF signals. The curves labeled “Mag” in Fig. 12a and Fig. 12b are the distributions of the top 10% largest or smallest DTW distances between any two geomagnetic signal segments collected at the same location or different locations, respectively. We can see that among these worst cases, the same-location DTW distances are significantly larger than the different-location DTW distances,

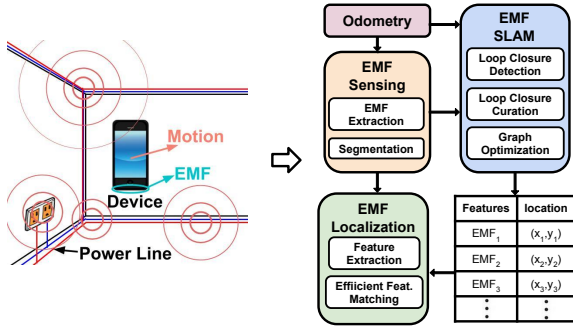


Figure 13: System workflow.

undermining the recall and precision performance in location identification. The curves labeled “micEMR” are the corresponding results obtained using the 100 Hz powerline EMR harmonic sensed by the P9’s microphone. Although the micEMR’s two distributions overlap, the micEMR’s recall and precision performance will be clearly better than the geomagnetism’s. The “Mag+micEMR” curves are the corresponding results using the average of the Mag-based and micEMR-based DTW distances. The above results show that, on smartphone platforms, power network EMF and geomagnetism can be complementary in discriminating locations. A combination of geomagnetism and power network EMF can mitigate inefficacy of sole geomagnetism-based location sensing.

Power Consumption of Power Network EMF Sensing:

According to the study [40], the power consumption of sampling microphone is low. On the other hand, the plethora of acoustic-based virtual assistants on smartphones and wearables (e.g., Apple Siri [37]) also require the microphones to be always on. Therefore, in practice, our proposed approach can leverage the audio data collected by these virtual assistants, without incurring excessive energy consumption.

4 SLAM WITH POWER NETWORK EMF

Based on the understanding obtained in §3, this section develops a novel **Simultaneous Localization And Mapping (SLAM)** approach with the power network EMF. As discussed above, power network EMF tends to exhibit better temporal stability comparing to geomagnetism, while providing certain spatial discriminability. However unlike other modalities such as vision, loop closures candidates obtained by directly comparing the power network EMF signal similarities often contain many false positives, which could significantly degrade the SLAM performance. To address this, the proposed SLAM approach employs novel loop closure detection and curation algorithms, which are able to discover as many potential loop closures as possible based on the sequential power network EMF measurements, while robustly rejecting

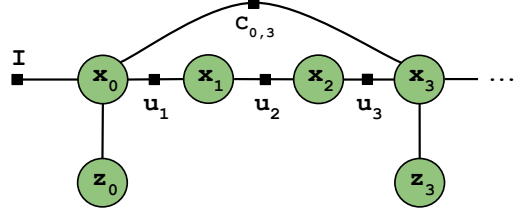


Figure 14: Factor graph representation for EMF-SLAM. x is the hidden state of actual user position; z denotes the power network EMF measurement; c is the loop closure of same place.

the false positive loop closure proposals by checking their spatial consistency.

Fig. 13 illustrates the workflow of our SLAM and localization approaches. Specifically, the sensed power network EMF signals are bandpass-filtered to extract the 50/60Hz signal and its harmonics. By using a dead-reckoning module on the motion data of the user, her trajectories/odometry is estimated. The filtered power network EMF signal is then segmented into sequences based on footsteps estimated in odometry information. The power network EMF sequences and odometry are sent to the loop closure detection module to first detect the revisited positions by the user. The detected loop closures are then curated to remove false positives in them. By using the SLAM algorithms with the estimated odometry and curated loop closures, the accurate trajectories of users can be recovered. By looking back the timestamp of the recovered locations and their associated power network EMF signatures, a feature map can be constructed. New users’ location can be predicted via matching their power network EMF readings with the feature map, even if their odometry information is not available. Note that this SLAM approach is fundamentally different from the standard fingerprinting. In our case, the feature map is automatically constructed as users move across the space, rather than manually collected through the labor-intensive fingerprinting process, which requires the users to explicitly establish the correspondence between specific locations and their EMF features. In addition, our SLAM approach can continuously improve and enrich the EMF feature map as the users explore the space more, e.g. in different walking directions, and eventually obtain a holistic view of the EMF signatures of the environment.

In what follows, we first present the problem formulation using the Graph SLAM machinery [26] in §4.1, and then discuss the proposed loop closure detection and curation algorithms in §4.2-§4.3. Finally, §4.4 provides an efficient online localization scheme using the constructed power network EMF feature maps.

4.1 Graph SLAM Formulation

States, Measurements and Outputs: Fig. 14 shows the factor graph representation of our SLAM formulation. Let \mathbf{x}_t denote the hidden *state*, i.e., actual position of the user in the workspace at discrete timestamp t . We assume that at each t , the user observes a *power network EMF measurement* \mathbf{z}_t , which contains the sequence of power network EMF signals received within a window $[t - \tau, t]$. Note that here we consider a signal sequence rather than point as the measurement because as shown in §3.1, longer power network EMF signal sequences tend to have more spatial discriminative power. We also assume that the relative displacement between two user positions \mathbf{x}_t and \mathbf{x}_{t-1} is captured by an odometry edge \mathbf{u}_t , e.g., estimated with PDR techniques. In practice, we often assume the initial location of the user (starting state I) can be known through other sources [26], e.g., CCTVs or card swipe systems at the entrance of the venue. After the user finishes traversing the workspace, the SLAM module should output the estimated sequence of true locations of the user $\mathbf{x}_0, \dots, \mathbf{x}_T$, along with the power network EMF feature map, which can be obtained by associating the observed power network EMF measurements $\mathbf{z}_0, \dots, \mathbf{z}_T$ with the state sequence.

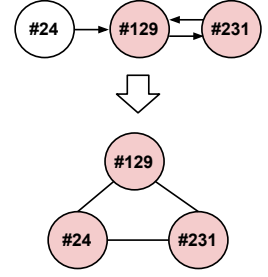
Loop Closure using Power Network EMF Signals: In a typical SLAM setting, loop closure refers to the recognition of when the user or agent has returned to a previously visited location, e.g., via observing similar measurements. It is one of the key components of SLAM framework, since in most cases, odometry measurements tend to be noisy, resulting in unbounded errors in state and map estimation. For instance, our system uses a PDR module which relies on the low-cost IMUs on mobile devices to estimate odometry, and inherently suffers from drift. Loop closure on the other hand, can enforce constraints (often on distance) between states, e.g., \mathbf{x}_0 and \mathbf{x}_3 in Fig. 14 are connected by an edge $c_{0,3}$, indicating that they should represent the same location in the workspace. This immediately reduces the uncertainty in state and map estimation, and therefore, the quality of detected loop closures has a direct impact on SLAM performance. In this work, we exploit the similarity between features at 50Hz of the observed power network EMF measurements to detect loop closures. As shown later, by carefully designing detection and curation algorithms, the power network EMF signals can be used to generate effective and robust loop closures across the workspace.

Graph Optimization: Given the odometry and loop closures, the optimal state sequence $\mathbf{X}^* = \{\mathbf{x}_0^*, \dots, \mathbf{x}_T^*\}$ can be estimated by solving:

$$\mathbf{X}^* = \underset{\mathbf{X}}{\operatorname{argmin}} \sum_i \underbrace{\|f_u(\mathbf{x}_i, \mathbf{u}_i) - \mathbf{x}_{i+1}\|_{\Sigma_i}^2}_{\text{odometry constraints}} + \sum_{\langle i, j \rangle} \underbrace{\|f_c(\mathbf{x}_i, \mathbf{c}_{ij}) - \mathbf{x}_j\|_{\Lambda_{ij}}^2}_{\text{EMF loop closure constraints}}$$

Timestamp	Closest-point timestamp	Closest-point distance
1	42	0.94
...
24	129	0.21
...
58	280	0.25
...
129	231	0.18
...
231	129	0.18
...
280	58	0.25
...

(a) CPP



(b) Proposal merging

Figure 15: Illustration example of closest-point profile (CPP) and loop-closing proposals. (a) Color-shaded fields are primary loop closures and the transparent field is a subsidiary one. (b) Merging primary and subsidiary loop-closing proposals. Nodes in the graph are proposal nodes, and edges are proposed loop closures.

where $f_u(\mathbf{x}_i, \mathbf{u}_i)$ describes the user motion reported by odometry, with uncertainty characterized by covariance matrix Σ_i . $f_c(\mathbf{x}_i, \mathbf{c}_{ij})$ is the loop closure model, and in this paper we use co-location with zero displacement, i.e., $f_c(\mathbf{x}_i, \mathbf{c}_{ij}) = \mathbf{x}_j$, and the covariance is Λ_{ij} .

4.2 Loop Closure Detection

This section presents the proposed approach of detecting loop closures using power network EMF signals.

Distance between Measurements: One key prerequisite for any loop closure approach is the distance metric between the measurements. In our context, a power network EMF measurement contains a sequence of power network EMF signals. To account for different walking speed of the users, when comparing two measurements \mathbf{z}_t and $\mathbf{z}_{t'}$, we use dynamic time warping (DTW) to align them, i.e. we first stretch the two sequences and then use the smallest sum of the Euclidean distances between their corresponding points as the distance metric. For each newly observed measurement \mathbf{z}_t , we compute its distance with respect to all previous measurements, and maintain the pairwise distance between them in a matrix \mathbf{Q} .

Closest Point Profile (CPP): Given the current \mathbf{Q} , we try to discover loop closures, i.e., measurements that are similar to each other and likely to represent the same locations. Instead of directly working with \mathbf{Q} , we firstly derive a *closest point profile* (CPP) representation, where for each measurement we only keep the timestamp of its closest peer and their distance. For instance, the entry (129, 213, 0.18) in Fig. 15 means that for measurement \mathbf{z}_{129} , the closest measurement (i.e., most similar one) observed so far is \mathbf{z}_{231} , and their distance is 0.18 under the distance metric discussed above. Note

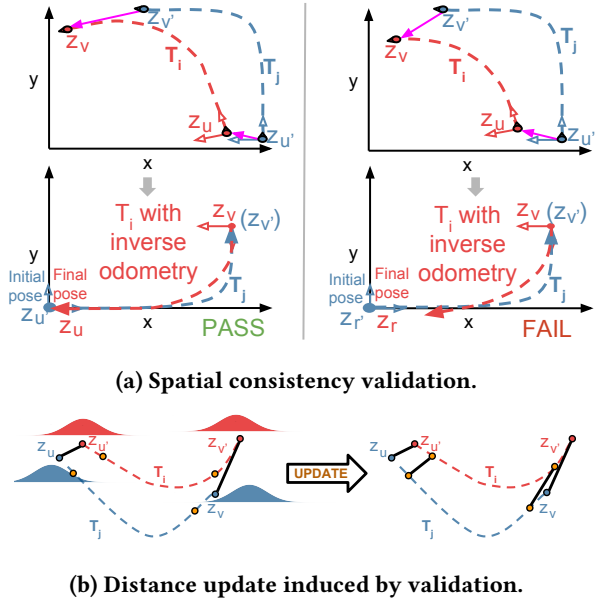


Figure 16: An example of loop closure curation.

that, in practice, CPP may not necessarily be symmetric under the distance metric. For example, as in Fig. 15, the closest peer of z_{24} is z_{129} , but for z_{129} , z_{24} is not the closest.

Mining Loop Closure Proposals from CPP: Intuitively, the entries in CPP are potential loop closures, each of which represents the local best knowledge on closest measurements and associated distances. Like most of the existing SLAM approaches, we could just naively threshold the distance, and propose the top- k entries with smallest distances as loop closures. However, in practice, such a technique is not robust to noise, and could propose many false positives. In this paper, we consider a new approach exploiting the graph structure of CPP. Concretely, we first discover the symmetric entries within CPP, e.g., as shown in Fig. 15, both z_{129} and z_{231} treat each other as the closest peer. The rationale is that, regardless of the absolute distances, the fact that both measurements confirm each other as the closest indicates that they are likely to observe the same landmark. Therefore, we initialize the set of loop closure proposals using those symmetric entries. To harvest more potential loop closures, we also add entries whose 2-nearest neighbours are symmetric, e.g., entry (24, 129, 0.21) in Fig. 15(b) will be included in the loop closure proposal set, since measurement z_{129} appears in an symmetric entry.

4.3 Loop Closure Curation

Given the set of loop closure proposals, in theory, we could use all of them to directly optimize the graph and solve the SLAM problem (as in §4.1). However, in practice, the SLAM framework can be very sensitive to false positives,

i.e., even a small amount of erroneous loop closures would greatly deteriorate graph optimization, and have a knock-on effect on its performance. To address this, we propose a loop closure curation approach, and exploit the spatial consistency to reject false positives and iteratively discover new valid proposals.

Spatial Consistency Validation: In our context, a true loop closure contains a pair of measurements which observe the same landmark in the workspace, although they may be captured at different timestamps or even by different users. Consider two loop closure proposals, involving two pair of measurements as ($z_u, z_{u'}$) and ($z_v, z_{v'}$) as shown in Fig. 16a(left). In this case, if both loop closures are true, then within any consistent reference frame, the two trajectory segments T_i and T_j defined by the four measurements will form a *loop*, since z_u and $z_{u'}$, z_v and $z_{v'}$ should be observed in the same locations. Consider the 2D Euclidean reference frame where $z_{u'}$ is positioned at the origin (0, 0). Conceptually, if we move from $z_{u'}$ (at the origin) to $z_{v'}$ using the odometry information encoded in T_j , hop to z_v via the loop closure link from $z_{v'}$, and then traverse back according to the *reverse* odometry in T_i , when reaching measurement z_u we should be able to return to the origin. This is because z_u and $z_{u'}$ should correspond to the same landmark. If this is the case, we confirm that both loop closure proposals are true, and mark them as valid (ready to be used by the later graph optimization). On the other hand, if we fail to return to the origin, e.g., as shown in Fig. 16a(right), then at least one of the two loop closure proposals is false positive. In that case we will not push any of them to later optimization, and temporarily keep them in the proposal set for next validation.

Distance Update Induced by Validation: As discussed above, if two loop closure proposals pass the the spatial consistency validation, we believe that the two trajectory segments (see T_i and T_j in Fig. 16b) would share the same start and end locations in the workspace (z_u and $z_{u'}$, z_v and $z_{v'}$ in Fig. 16a(left)). On the other hand, this also indicates that measurements within the neighbourhood of those validated loop closures should be spatially close, and there might still be valid loop closures missed by the previous detection algorithm. To exploit this constraint, we update the pairwise distances of those measurements within that neighborhood.

Concretely, given the validated loop closure containing two measurements z_u and $z_{u'}$ ($z_u \in T_i$, $z_{u'} \in T_j$), we first consider the neighborhood of $2N + 1$ measurements around z_u and $z_{u'}$ respectively, i.e., two sequences of measurements $\{z_{u-N}, \dots, z_{u+N}\}$ and $\{z_{u'-N}, \dots, z_{u'+N}\}$. The size of N is determined by the shape similarity of the two trajectory segments T_i and T_j : $N \propto 1/DTW(T_i, T_j)$, where $DTW(T_i, T_j)$ is the DTW distance based on odometry information. For

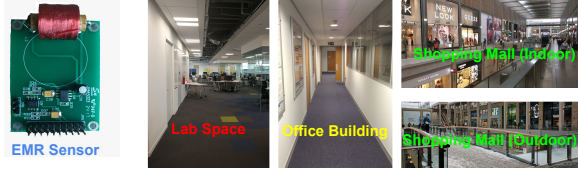


Figure 17: Powerline EMR sensor and test venues.

the $2N + 1$ window, we define a Gaussian kernel: $w(n) = e^{-\frac{1}{2}(Q(z_u, z_{u'}) - \frac{n}{N})^2}$, where $-N \leq n \leq N$, and $Q(z_u, z_{u'})$ is the distance between measurements z_u and $z_{u'}$ of the validated loop closure. Then for each pair of measurements $z_{u+n} \in T_i$ and $z_{u'+n'} \in T_j$ ($-N \leq n, n' \leq N$) between the two $2N + 1$ windows, we update their distance as follows:

$$Q^{new}(z_{u+n}, z_{u'+n'}) = Q(z_{u+n}, z_{u'+n'}) - \beta \cdot w(n) \cdot Q(z_u, z_{u'}).$$

Here, $Q(z_{u+n}, z_{u'+n'})$ is the current distance, and β is the updating rate which controls how much distance change should be applied.

Iterative Loop Closure Curation: With the updated Q , where measurements around the validated loop closures have new distance values, we then drive the detection algorithm to discover any new loop closure proposals. This detection-validation cycle runs iteratively: in each iteration we first discover loop closure proposals, validate them, and finally use the validation results as constraints to update our previous belief on distances between measurements, which is then used by the loop closure detection algorithm in the next iteration. This loop closure curation process continues, until there is no proposal can satisfy the spatial consistency validation. In this way, our system is able to discover as many genuine loop closures as possible, and as shown later in the evaluation, it is the key for our SLAM framework to build accurate and consistent power network EMF feature maps.

4.4 Efficient Real-time Localization

In essence, the proposed SLAM framework leverages the odometry information and power network EMF, to jointly estimate the location of the user and the power network EMF feature map of the workspace within a metrically consistent frame of reference. In practice, this process typically happens offline in the cloud, since it requires optimization over all states and measurements (as discussed in §4.1). On the other hand, if the power network EMF feature map of the workspace has been constructed using the proposed SLAM approach (e.g., via crowdsourcing), we could position the user directly with respect to the map. In the following, we show that such localization can be achieved in real-time on resource-constrained devices without infrastructure support: once the power network EMF feature map is downloaded

to the user’s mobile device, she can be localized using the carried device only.

Localization with Power Network EMF Feature Map:

Assume that the workspace is a 2D *discrete* Euclidean space, and has been thoroughly surveyed by our SLAM approach. In this case, the produced power network EMF feature map can be viewed as a 2D grid, where each grid represents a location l and the associated power network EMF signature \bar{z}_l . In this paper, \bar{z}_l is defined as the DTW centroid [30, 31] of all power network EMF measurements observed at location l , which is also a sequence of power network EMF signals. Therefore, localization with respect to the feature map can be cast into a classification problem, where for a live power network EMF measurement z_t , we try to find the location that has the closest power network EMF signature. In our context, we consider a similar distance metric as in §4.2, which employs DTW to evaluate the similarity between power network EMF signal sequences. However, unlike in SLAM (see §4.2) where we only use power network EMF features at 50 Hz for robustness, during localization we consider three frequency components 50 Hz, 100 Hz and 150 Hz (the harmonics), to exploit more discriminative power of power network EMF signals. Therefore, the distance between the live power network EMF measurement z_t and the power network EMF signature at a given location is evaluated as the weighted sum of distances between signals at the three frequency components, where weights are learned from the data. Finally, given the pairwise distances between live power network EMF measurement z_t and power network EMF signatures at different locations, the estimated location is given by a Nearest Neighbour (NN) classifier.

Sparse Power Network EMF Feature Analysis: The above localization scheme is intuitive and easy to implement, but may incur substantial computational cost since a newly observed power network EMF measurement has to be compared against power network EMF signatures of all locations within the feature map, where each comparison involves one run of DTW. This would pose significant negative effect on performance when feature maps become bigger/denser, or for resource constrained devices such as wearables. To address this, we propose a sparse power network EMF feature analysis approach which only works on much sparser power network EMF signals to speed up processing. The intuition is that within a short period, the power network EMF signals tend to *smooth* with low variance, i.e., most values are entered around the sample mean. Therefore, when comparing a given measurement z_t with the power network EMF signatures in the feature map, we first use the mean values to filter out those locations whose mean power network EMF signatures are very far away from that of z_t . In our experiments, we find that this pre-processing step is very

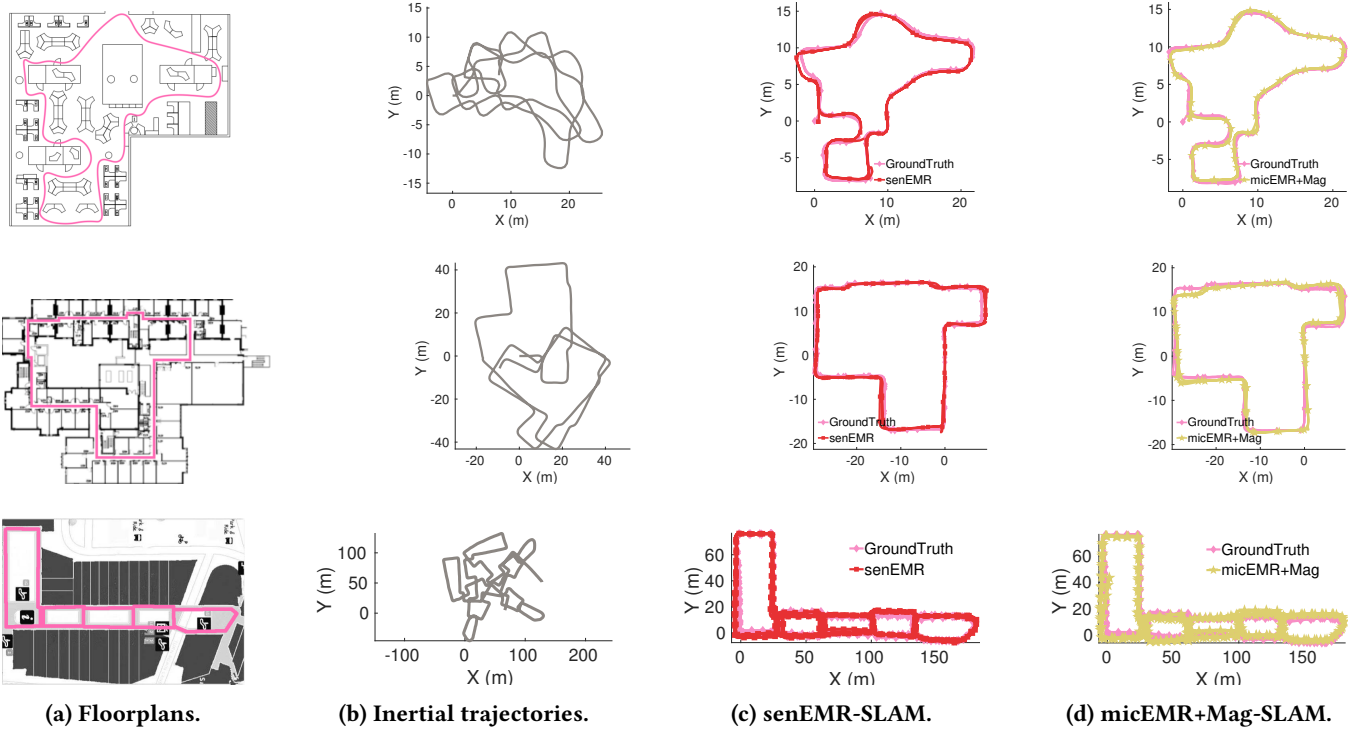


Figure 18: Floorplans (a), inertial trajectories produced by PDR (b), and the maps estimated by the proposed senEMR-SLAM (c) and micEMR+Mag-SLAM (d) in lab (top), office building (middle) and shopping mall (down).

effective: on average it can rule out about 90% of locations in the feature map, with less than 2% drop in overall localization accuracy. In addition, given the sample mean $\mu(\mathbf{z}_t)$ and variance $\sigma(\mathbf{z}_t)$ of a power network EMF measurement \mathbf{z}_t , the signal sequence encoded in \mathbf{z}_t can be sparsified by collapsing all values within $[\mu(\mathbf{z}_t) - \lambda\sigma(\mathbf{z}_t), \mu(\mathbf{z}_t) + \lambda\sigma(\mathbf{z}_t)]$ as zeros. λ is the sparsity factor, which controls how much information would be omitted from the original signal. The resulting consecutive zeros are then clustered together, and we only keep the lengths of them in the sequence. We apply the same process to the power network EMF signatures, and then run DTW on the sparse representations, which should be much shorter than the original signals. The rationale is that we have already used mean values to compare \mathbf{z}_t with the power network EMF signatures, and thus values close to its mean won't be able to contribute further information. As shown later in the evaluation, this sparse analysis approach can significantly reduce computation latency of localization.

5 EVALUATION

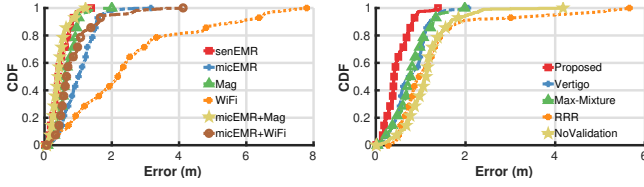
5.1 Experiment Setup

Sites: We evaluated the performance of proposed power network EMF-based SLAM and localization approaches in three venues across two countries, including (i) an office building

(1,750 m²), which was built over 20 years ago with stones and bricks, and reinforced with metal rebars; (ii) a semi-outdoor shopping center (11,000 m²) built recently close to a highway; and (iii) a lab space (900 m²) in another country, which has the same 50Hz powerline frequency but different layout. Fig. 17 shows the snapshots of these test venues.

Sensing Modalities and Platforms: In our experiments we employed a variety of sensing modalities, and collected the following data: (i) power network EMF signals from a customized powerline EMR sensor as shown in Fig. 17, (ii) audio from microphones, (iii) geomagnetic field from the smartphone magnetometer, and (iv) WiFi RSS on smartphones. We used 5 devices with different specs, including Raspberry Pi 2 and 3, Galaxy S7, Huawei P9, and Nexus 6.

Data Collection Protocol: We recruited 10 participants with different heights (1.58m to 1.88m), and asked them to hold the devices and walk normally in the experiment sites. We collected about 5 hours of walking data in total from the three sites, where longer trajectories with multiple loops are used to evaluate the proposed SLAM approach, while the rest for localization. We employ Google Tango tablet [24] to obtain ground truth for both user trajectories and constructed feature maps. The visual-inertial odometry is fused with manually inserted loop closures using visual SLAM [19].

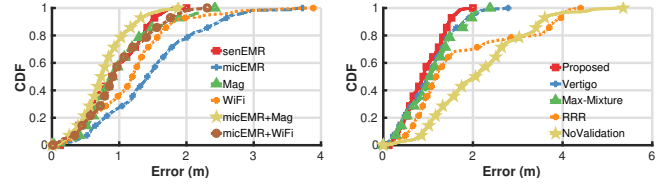


(a) Sensing modality (b) Validation method
Figure 19: SLAM performance in the lab space.

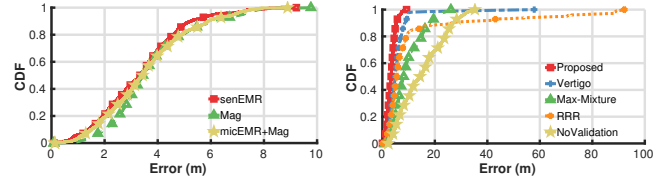
5.2 Experiment Results

Effectiveness of SLAM using Power Network EMF: The first experiment studies the effectiveness of SLAM using power network EMF. We refer to the SLAM approach using power network EMF sensed via the customized receiver as *senEMR-SLAM*, while via microphone as *micEMR-SLAM*. The two proposed approaches are compared against: (i) *WiFi-SLAM* and (ii) *Mag-SLAM*, which use WiFi RSS [11, 50] and earth geomagnetic field [12, 44] for SLAM. Fig. 18 shows the floorplans (a), the inertial trajectories produced by PDR (b), and the maps (shown as trajectories) estimated by the proposed *senEMR-SLAM* (c) and *micEMR+Mag-SLAM* (d) across three experiment sites. We see that in all sites both approaches can produce much more consistent trajectories than PDR, which are very similar to the ground truth. Fig. 19(a), 20(a) and 21(a) further show the error distributions of maps constructed by different SLAM approaches using a variety of sensing modalities. As we can see, *senEMR-SLAM* consistently outperforms the other single-modality SLAM approaches, and can reach 0.42m accuracy for 90% of the time in the lab space, while achieving 3.34m mean accuracy in the very challenging shopping center. On the other hand, *Mag-SLAM* has about 15% more error than *senEMR-SLAM*, while *WiFi-SLAM* performs even worse. Although both exploit the power network EMF, the performance of *micEMR-SLAM* is generally inferior to *senEMR-SLAM* due to the background noise in audio data. This is expected, however in the lab space *micEMR-SLAM* is still better than *WiFi-SLAM* (Fig. 19(a)). In the challenging shopping center, neither *micEMR-SLAM* nor *WiFi-SLAM* is able to construct a reasonable map (errors not shown in Fig. 21(a)). On the other hand, when fused with other sensing modalities, e.g. *micEMR-SLAM* + *Mag-SLAM*, the SLAM accuracy could improve by 20% on average than *Mag-SLAM* alone.

Performance of Iterative Loop Closure Curation: This experiment investigates the performance of the proposed iterative loop closure curation algorithm. We compare our approach with the state-of-the-art loop closure checking algorithms: (i) *RRR* [21] which identifies valid loop closures by clustering them; (ii) *Max-mixture* [28] which employs a mixture model to capture probabilities of valid loop closures;



(a) Sensing modality (b) Validation method
Figure 20: SLAM performance in the office building.



(a) Sensing modality (b) Validation method
Figure 21: SLAM performance in the shopping center.

and (iii) *Vertigo* [39], which uses latent variables to model the validity of loop closures. We also include the baseline *No Validation*, which naively pushes all loop closure proposals to optimization without any validation. Fig. 19(b), 20(b) and 21(b) shows the error CDF of different approaches. Firstly, we see that loop closure validation is a necessary step, and can significantly improve SLAM accuracy: in the shopping center, the proposed approach can reduce the error to 20% (from 15.06m to 3.34m), compared to no validation. Comparing to other loop closure validation techniques, our approach can achieve approximately 1.5-fold reduction in error and the accuracy degrades gracefully. This is because our approach is able to iteratively validate and mine genuine loop closures, while the competing ones just run one-off validation.

Localization Accuracy: Now we evaluate the online localization accuracy of different modalities given their constructed feature maps. Intuitively, the performance of localization depends very much on the quality of maps registered by SLAM. Therefore in this set of experiments we only consider the lab and office settings, because feature maps estimated by single modalities (*senEMR*, *micEMR*, *Mag* or *WiFi-SLAM*), even the best ones, have non-negligible errors, and it does not make sense to evaluate localization accuracy with respect to them. Similarly, we only compare the proposed power network EMF based localization approaches (*senEMR-Loc* using the customised receiver, and *micEMR-Loc* using microphones) with magnetic field based approach (*Mag-Loc*) since *WiFi* does not perform well. Fig. 22 shows the CDF of localization accuracy. As we can see, *senEMR-Loc* outperforms the other approaches, achieving mean accuracy of 1.59m in the lab space and 3.93m in the office building. Note that *Mag-Loc* performs particularly bad on the lab space (see. Fig. 22(a)). This is because we use data collected from

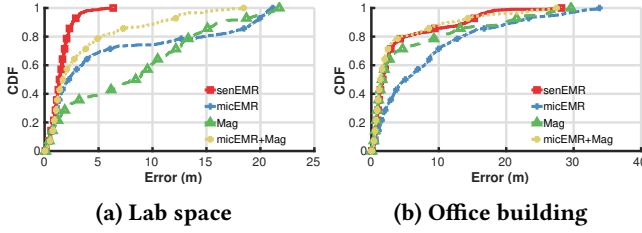


Figure 22: Localization performance of different sensing modalities.

a participant of height 162cm to build the magnetic feature map, while tried to localise another of 190cm. This confirms that magnetism based approaches are not robust to height, while the proposed power network EMF based approaches do not suffer from this problem. On the other hand, using only power network EMF sensed via microphones (micEMR-Loc) has generally larger errors than that of using customized receivers (senEMR-Loc). However, when fused with magnetic field (micEMR+Mag-Loc), the localization errors could be halved comparing to the single best modality: from 8.2m (micEMR-Loc only) to 3.7m in the lab space and 8.4m (Mag-Loc only) to 3.9m in the office building.

Sensitivity to Power Network EMF Sequence Length: This experiment looks into the sensitivity of localization performance with respect to the sequence length of power network EMF signals included in one measurement. We consider two realistic settings: (i) running senEMR-Loc on Raspberry Pi (RP2 and RP3), which can be used in various IoT applications; and (ii) running micEMR+Mag-Loc (fusion of micEMR-Loc and Mag-Loc) on smartphones, which provides an alternative option for infrastructure-free positioning. As shown in Fig. 24 and 25, we vary the length of power network EMF signals in terms of steps: e.g. 2-step means in a power network EMF measurement we include signals observed within the last 2 steps. We see that senEMR-Loc and micEMR+Mag-Loc achieve comparable localization accuracy: generally longer sequences result in better accuracy, while the gaps become marginal when the sequence length is bigger than 6-step. For instance, for both senEMR-Loc and micEMR+Mag-Loc, using signals of 10-step would only improve localization accuracy by $<0.2\text{m}$ comparing to 6-step. On the other hand, longer sequences take more time to process, e.g. using 10-step would significantly increase localization time as shown in Fig. 24 and 25 (up to $\sim 3\text{s}$ for one measurement), which is not cost-effective.

Performance Gain by Sparse Feature Analysis: The last set of experiments verify the impact of the proposed sparse feature analysis on localization performance. We use the same two settings (that is, senEMR-Loc on Raspberry Pi, and

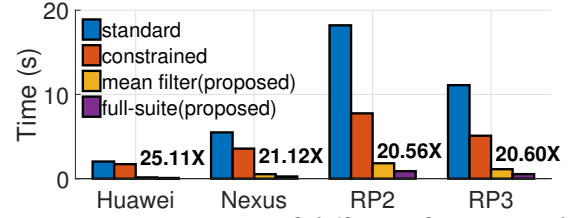


Figure 23: Running time of different feature analysis approaches on test devices.

Table 1: Localization accuracy (m) of different feature analysis approaches.

	raw DTW	constrained	mean filter	full
senEMR	1.76	1.89	1.77	2.01
micEMR + Mag	4.15	5.58	4.20	4.71

micEMR+Mag-Loc on smartphone) as in the previous experiment, and compare the proposed sparse feature analysis approach (in §4.4) with: (i) standard DTW, (ii) constrained-DTW [27] which imposes local constraints on searching when aligning sequences, and (iii) a straw man version of the proposed approach, using mean filter only to pre-select matching sequences. For the proposed approach, we temporarily fix the sparsity level (controlled by λ in §4.4) to 25%. This means that during sparse feature analysis, 25% of values in the original signal would be set to zero since they are close to the mean. Fig. 23 shows the wall-clock running time of different approaches, and the resulting localization accuracy is shown in Tab. 1. We see that even with mean filter only, we can already run $\sim 10\times$ faster than standard-DTW, while the drop in accuracy is negligible. On the other hand, the full version of proposed sparse feature analysis approach can achieve up to $25\times$ performance gain in running time compared to standard-DTW, at the cost of $\sim 15\%$ accuracy loss, which is still comparable with the state-of-the-art (constrained-DTW). When we vary the sparse level (from 0% to 50% as shown in Fig. 24, we observed that sparser signals take shorter time to process ($\sim 0.1\text{s}$ less per 5% on RP3), while resulting in negligible increase in localization error ($\sim 0.06\text{m}$). This confirms that the proposed sparse feature analysis approach can achieve desire trade-off between cost and accuracy. In particular, as in Fig. 24, when using 25% sparsity and 6-step power network EMF signals, it takes 0.69s to process one measurement, which is within the time for one footstep. Therefore, we could run real-time power network EMF based localization on the resource constrained Raspberry Pi with reasonable accuracy.

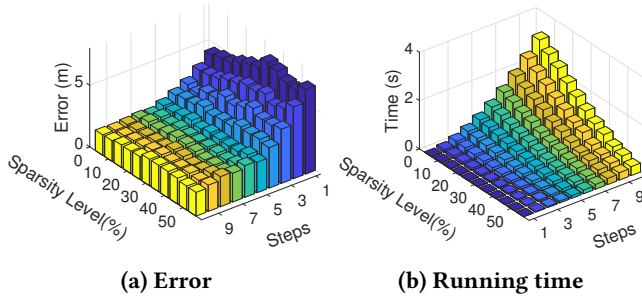


Figure 24: Accuracy and running time on RP3.

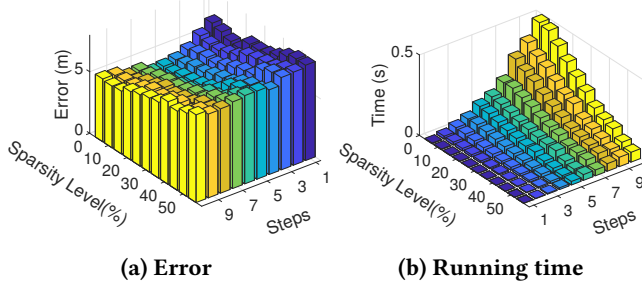


Figure 25: Accuracy and running time on Huawei P9.

6 RELATED WORK

As discussed in §1, recent studies [23, 33, 48] have exploited powerline EMR for time-related services. In [29, 38], modulated high-frequency signals are injected into a building’s power network and then the corresponding power network emanations are sensed by a mobile device equipped with an EMR sensor for localization. However, the requirements of one or more signal injectors and intensive *in situ* training introduce significant system deployment overhead. The Humantenna system presented in [9] uses the human body as an antenna to receive powerline EMR and recognize gestures. Preliminary results on recognizing the user’s location among pre-spotted locations are presented. However, the physical connection with the user’s body and system training bring overheads. To the best of our knowledge, this paper presents the first work on using power network EMF measurements captured by a standalone sensor or smartphone for SLAM and localization.

Originally designed for robotics, SLAM has been applied to mobile computing applications [3, 43]. However, due to mobile devices’ low-cost and noisy IMUs and human’s complicated motion patterns, SLAM for human-centric applications is often challenging. Early solution [11, 50] use WiFi RSS and IMUs for SLAM. However, WiFi RSS suffers from the multi-path effects and the performance of SLAM degrades significantly in dynamic environments, e.g., retail stores. Geomagnetism-based SLAM is recently introduced [12, 18, 44]. However, geomagnetism often exhibits high

variability with altitude. Recent SLAM systems also leverage vision techniques [10, 14], which raise privacy concerns [52], however. Our SLAM system differs from the above systems in its new sensing modality – power network EMF – that exhibits desirable high repeatability. Our system also features a bespoke approach that detects power network EMF loop closures reliably and produces better SLAM results.

Localization can be seen as a special case of SLAM where the map is known or obtained through SLAM. Existing localization approaches can be divided into two categories. First, *model-based* approaches estimate the distance between a user device and deployed anchors based on models of RSS [5, 7], angle of arrival [20, 46], or propagation time [25, 42, 45]. However, non-line-of-sight conditions often degrade the performance of these approaches. Differently, powerline EMR with extremely long wavelengths can well penetrate barriers. Second, *fingerprinting* approaches develop a map of features extracted from images [13, 54], sounds [41], geo-magnetic field [22, 35, 36], RF signals [6, 51], visible lights [49, 52, 55] and a mix of them [4, 34, 47]. However, these approaches generally require a laborious blanket process of (re-)fingerprinting all locations. Owing to the temporal stability of power network EMF, our approach requires a one-shot profiling only, coinciding with the concept of *light registration* [53]. Moreover, the profiling can be accomplished via crowd-sourced SLAM in an unsupervised manner.

7 CONCLUSION

This paper systematically investigated the spatial distinctness and temporal stability of EMFs induced by buildings’ power networks. Based on the result, we designed a SLAM approach that can reliably detect loop closures with power network EMF signals sensed by either a customized receiver or a smartphone’s microphone as a side-channel sensor. Moreover, with the power network EMF feature map constructed by SLAM, we design an efficient localization algorithm that can position the user in real time on resource-constrained devices. Our extensive evaluation shows that the power network EMF is a promising modality for indoor location sensing since it is ubiquitous, spatially distinct, temporally stable, and noise resilient. By exploiting these advantages of power network EMF, the proposed SLAM and localization approaches are capable of achieving sub-meter accuracy, while run in real time on both smartphones and embedded hardware. Advanced approaches for fusing power network EMF measurements with the measurements in other sensing modalities, as well as 3D indoor localization with power network EMF are interesting topics for future work.

REFERENCES

- [1] [n. d.]. Carrier Current Radio Systems. ([n. d.]). <http://www.radiosystems.com/carriercurrent.html>.
- [2] [n. d.]. Greenlee Circuit Seeker. ([n. d.]). <http://bit.ly/2tzf6EL>.
- [3] Heba Abdelnasser, Reham Mohamed, Ahmed Elgohary, Moustafa Farid Alzantot, He Wang, Souvik Sen, Romit Roy Choudhury, and Moustafa Youssef. 2016. SemanticSLAM: Using environment landmarks for unsupervised indoor localization. *IEEE Transactions on Mobile Computing* (2016).
- [4] Martin Azizyan, Ionut Constandache, and Romit Roy Choudhury. 2009. SurroundSense: mobile phone localization via ambience fingerprinting. In *ACM MobiCom*.
- [5] Paramvir Bahl and Venkata N Padmanabhan. 2000. RADAR: An in-building RF-based user location and tracking system. In *IEEE INFOCOM*.
- [6] Yin Chen, Dimitrios Lymberopoulos, Jie Liu, and Bodhi Priyantha. 2012. Fm-based indoor localization. In *ACM MobiSys*.
- [7] Krishna Chintalapudi, Anand Padmanabha Iyer, and Venkata N Padmanabhan. 2010. Indoor localization without the pain. In *ACM MobiCom*.
- [8] Jaewoo Chung, Matt Donahoe, Chris Schmandt, Ig-Jae Kim, Pedram Razavai, and Micaela Wiseman. 2011. Indoor location sensing using geo-magnetism. In *Proceedings of the 9th international conference on Mobile systems, applications, and services*. ACM, 141–154.
- [9] Gabe Cohn, Daniel Morris, Shwetak Patel, and Desney Tan. 2012. Humantenna: using the body as an antenna for real-time whole-body interaction. In *Proceedings of the SIGCHI Conference on Human Factors in Computing Systems*. ACM, 1901–1910.
- [10] Jakob Engel, Thomas Schöps, and Daniel Cremers. 2014. LSD-SLAM: Large-scale direct monocular SLAM. In *European Conference on Computer Vision (ECCV)*.
- [11] Brian D Ferris, Dieter Fox, and Neil Lawrence. 2007. WiFi-SLAM using Gaussian process latent variable models. In *AAAI*.
- [12] Chao Gao and Robert Harle. 2015. Sequence-based magnetic loop closures for automated signal surveying. In *Indoor Positioning and Indoor Navigation (IPIN), 2015 international conference on*.
- [13] Ruipeng Gao, Yang Tian, Fan Ye, Guojie Luo, Kaigui Bian, Yizhou Wang, Tao Wang, and Xiaoming Li. 2016. Sextant: Towards ubiquitous indoor localization service by photo-taking of the environment. *IEEE Transactions on Mobile Computing* (2016).
- [14] Ruipeng Gao, Bing Zhou, Fan Ye, and Yizhou Wang. 2017. Knitter: Fast, resilient single-user indoor floor plan construction. In *INFOCOM*.
- [15] Brandon Gozick, Kalyan Pathapati Subbu, Ram Dantu, and Tomyo Maeshiro. 2011. Magnetic maps for indoor navigation. *IEEE Transactions on Instrumentation and Measurement* 60, 12 (2011), 3883–3891.
- [16] Andreas Haeberlen, Eliot Flannery, Andrew M Ladd, Algis Rudys, Dan S Wallach, and Lydia E Kavraki. 2004. Practical robust localization over large-scale 802.11 wireless networks. In *Proceedings of the 10th annual international conference on Mobile computing and networking*. ACM, 70–84.
- [17] Jeffrey Hightower, Sunny Consolvo, Anthony LaMarca, Ian Smith, and Jeff Hughes. 2005. Learning and recognizing the places we go. In *International Conference on Ubiquitous Computing*. Springer, 159–176.
- [18] Jongdae Jung, Taekjun Oh, and Hyun Myung. 2015. Magnetic field constraints and sequence-based matching for indoor pose graph SLAM. *Robotics and Autonomous Systems* (2015).
- [19] Christian Kerl, Jurgen Sturm, and Daniel Cremers. 2013. Dense visual SLAM for RGB-D cameras. In *IEEE/RSJ International Conference on Intelligent Robots and Systems (IROS)*.
- [20] Manikanta Kotaru, Kiran Joshi, Dinesh Bharadia, and Sachin Katti. 2015. Spotfi: Decimeter level localization using wifi. In *ACM SIGCOMM*.
- [21] Yasir Latif, César Cadena, and José Neira. 2013. Robust loop closing over time for pose graph SLAM. *The International Journal of Robotics Research (IJRR)* (2013).
- [22] Liquan Li, Guobin Shen, Chunshui Zhao, Thomas Moscibroda, Jyh-Han Lin, and Feng Zhao. 2014. Experiencing and handling the diversity in data density and environmental locality in an indoor positioning service. In *ACM MobiCom*.
- [23] Yang Li, Rui Tan, and David KY Yau. 2017. Natural timestamping using powerline electromagnetic radiation. In *Proceedings of the 16th ACM/IEEE International Conference on Information Processing in Sensor Networks*. ACM, 55–66.
- [24] Eitan Marder-Eppstein. 2016. Project tango. In *ACM SIGGRAPH 2016 Real-Time Live!*
- [25] Alex T Mariakakis, Souvik Sen, Jeongkeun Lee, and Kyu-Han Kim. 2014. Sail: Single access point-based indoor localization. In *ACM MobiSys*.
- [26] Michael Montemerlo, Sebastian Thrun, Daphne Koller, Ben Wegbreit, et al. 2002. FastSLAM: A factored solution to the simultaneous localization and mapping problem. In *AAAI*.
- [27] Cory Myers, Lawrence Rabiner, and Aaron Rosenberg. [n. d.]. Performance tradeoffs in dynamic time warping algorithms for isolated word recognition. *IEEE Transactions on Acoustics, Speech, and Signal Processing* ([n. d.]).
- [28] Edwin Olson and Pratik Agarwal. 2013. Inference on networks of mixtures for robust robot mapping. *The International Journal of Robotics Research* (2013).
- [29] Shwetak N Patel, Khai N Truong, and Gregory D Abowd. 2006. Power-Line Positioning: A Practical Sub-Room-Level Indoor Location System for Domestic Use. *Lncs* 4206 (2006), 441–458. <https://doi.org/10.1007/11853565>
- [30] François Petitjean, Germain Forestier, Geoffrey I Webb, Ann E Nicholson, Yanping Chen, and Eamonn Keogh. 2014. Dynamic time warping averaging of time series allows faster and more accurate classification. In *IEEE International Conference on Data Mining (ICDM)*.
- [31] François Petitjean, Alain Ketterlin, and Pierre Gançarski. 2011. A global averaging method for dynamic time warping, with applications to clustering. *Pattern Recognition* (2011).
- [32] David Andrew Puts. 2005. Mating context and menstrual phase affect women’s preferences for male voice pitch. *Evolution and Human Behavior* (2005).
- [33] Anthony Rowe, Vikram Gupta, and Ragunathan Raj Rajkumar. 2009. Low-power clock synchronization using electromagnetic energy radiating from ac power lines. In *ACM SenSys*.
- [34] Guobin Shen, Zhuo Chen, Peichao Zhang, Thomas Moscibroda, and Yongguang Zhang. 2013. Walkie-Markie: Indoor pathway mapping made easy. In *USENIX NSDI*.
- [35] Yuanchao Shu, Cheng Bo, Guobin Shen, Chunshui Zhao, Liquan Li, and Feng Zhao. 2015. Magicol: Indoor localization using pervasive magnetic field and opportunistic WiFi sensing. *IEEE Journal on Selected Areas in Communications* (2015).
- [36] Yuanchao Shu, Kang G Shin, Tian He, and Jiming Chen. 2015. Last-mile navigation using smartphones. In *ACM MobiCom*.
- [37] Siri Team. 2017. Hey Siri: An On-device DNN-powered Voice Trigger for Apple’s Personal Assistant. (2017). <https://machinelearning.apple.com/2017/10/01/hey-siri.html>.
- [38] Erich P Stuntebeck, Shwetak N Patel, Thomas Robertson, Matthew S Reynolds, and Gregory D Abowd. 2008. Wideband powerline positioning for indoor localization. In *ACM Ubicomp*.
- [39] Niko Sünderhauf and Peter Protzel. 2012. Switchable constraints for robust pose graph SLAM. In *IEEE/RSJ International Conference on Intelligent Robots and Systems (IROS)*.
- [40] Sasu Tarkoma, Matti Siekkinen, Eemil Lagerspetz, and Yu Xiao. 2014. *Smartphone energy consumption: modeling and optimization*. Cambridge University Press.

- [41] Stephen P Tarzia, Peter A Dinda, Robert P Dick, and Gokhan Memik. 2011. Indoor localization without infrastructure using the acoustic background spectrum. In *ACM MobiSys*.
- [42] Deepak Vasisht, Swarun Kumar, and Dina Katabi. 2016. Decimeter-Level Localization with a Single WiFi Access Point.. In *USENIX NSDI*.
- [43] He Wang, Souvik Sen, Ahmed Elgohary, Moustafa Farid, Moustafa Youssef, and Romit Roy Choudhury. 2012. No need to war-drive: Unsupervised indoor localization. In *ACM MobiSys*.
- [44] Sen Wang, Hongkai Wen, Ronald Clark, and Niki Trigoni. 2016. Keyframe based large-scale indoor localisation using geomagnetic field and motion pattern. In *Intelligent Robots and Systems (IROS), 2016 IEEE/RSJ International Conference on*.
- [45] Yaxiong Xie, Zhenjiang Li, and Mo Li. 2015. Precise power delay profiling with commodity wifi. In *ACM MobiCom*.
- [46] Jie Xiong and Kyle Jamieson. 2013. Arraytrack: a fine-grained indoor location system. In *Usenix NSDI*.
- [47] Han Xu, Zheng Yang, Zimu Zhou, Longfei Shangguan, Ke Yi, and Yunhao Liu. 2016. Indoor localization via multi-modal sensing on smartphones. In *ACM Ubicomp*.
- [48] Zhenyu Yan, Yang Li, Rui Tan, and Jun Huang. 2017. Application-Layer Clock Synchronization for Wearables Using Skin Electric Potentials Induced by Powerline Radiation. In *SenSys*.
- [49] Zhice Yang, Zeyu Wang, Jiansong Zhang, Chenyu Huang, and Qian Zhang. 2015. Wearables can afford: Light-weight indoor positioning with visible light. In *ACM MobiSys*.
- [50] Zheng Yang, Chenshu Wu, and Yunhao Liu. 2012. Locating in fingerprint space: wireless indoor localization with little human intervention. In *ACM MobiCom*.
- [51] Moustafa Youssef and Ashok Agrawala. 2005. The Horus WLAN location determination system. In *ACM MobiSys*.
- [52] Chi Zhang and Xinyu Zhang. 2016. LiTell: robust indoor localization using unmodified light fixtures. In *MobiCom*. ACM.
- [53] Chi Zhang and Xinyu Zhang. 2017. Pulsar: Towards Ubiquitous Visible Light Localization. In *ACM MobiCom*.
- [54] Yuanqing Zheng, Guobin Shen, Liqun Li, Chunshui Zhao, Mo Li, Feng Zhao, Yuanqing Zheng, Guobin Shen, Liqun Li, Chunshui Zhao, et al. 2017. Travi-navi: Self-deployable indoor navigation system. *IEEE/ACM Transactions on Networking (TON)* (2017).
- [55] Shilin Zhu and Xinyu Zhang. 2017. Enabling High-Precision Visible Light Localization in Today's Buildings. In *ACM MobiSys*.